Determination of Dopant Density Profiles of Heavily Boron-Doped Silicon From Low Temperature Microphotoluminescence Spectroscopy

Young-Joon Han, Evan Franklin, Daniel Macdonald, Hieu T. Nguyen, and Di Yan

***Abstract*—Low temperature microphotoluminescence spectroscopy (μ-PLS) is employed to determine the inhomogeneous doping profiles for heavily boron-doped regions on silicon wafers. Samples having various Gaussian function doping profiles, in terms of surface dopant density and depth factor, are prepared via two-step thermal boron diffusion on high resistivity n-type silicon wafers. Measured PL spectra are normalized to the Si band–band luminescence peak, and PL components of undiffused Si are subtracted to resolve the doping peak. We show that the wavelength of the doping peak has a reliable and simple linear relationship with the measured surface dopant density on a semilog plot, and so establish a calibration curve which can be applied to estimate the surface dopant density. A second calibration curve for estimating the depth factor is also established after correcting the measured doping peak intensity to account for incomplete dopant ionization. We show the effectiveness of this method by reconstructing independently measured doping profiles using the surface dopant density and depth factors estimated from the PL spectra. Furthermore, by performing two-dimensional mapping, with μ-PLS measurements at 2 μm spatial resolution, we are able to map the surface dopant density and diffusion depth factor of micron-scale, locally diffused features.**

***Index Terms*—Doping profile, excitation spectroscopy, heavily doped silicon, photoluminescence.**

I. Introduction

ACCURATE characterization of the doped surface regions of silicon solar cells is critical for understanding and controlling electronic surface properties (recombination and contact properties) and thus optimizing the performance of high efficiency silicon solar cells. Localized features, for example, locally doped emitter and back surface field regions, as employed in various point contact solar cell concepts, are essential for achieving high conversion efficiency in many advanced silicon solar cell designs [1], [2]. Understanding the doping profile for such localized features is thus important, and it is desirable to have a reliable method for rapidly measuring and mapping the doping profile at the micron-scale. Common methods for measuring doping profiles include electrochemical capacitance–voltage (ECV) profiling [3], secondary-ion mass spectrometry [4], and inductively coupled plasma mass spectrometry [5]. These techniques can be used to accurately determine the density of dopant atoms as a function of depth. However, these techniques are destructive, and can only be applied on relatively large, uniformly doped regions. In this paper, we demonstrate that low-temperature microphotoluminescence spectroscopy (μ-PLS) can be employed to estimate nondestructively the key defining features of doping profiles for boron-doped samples, and furthermore can be used to perform two-dimensional (2-D) mapping of small, locally doped features.

PLS is a well-established characterization technique for silicon wafers and devices. The emitted spectra are influenced by a number of factors, including the presence of dopant impurities, thus making it possible to determine the dopant density quantitatively. Utilizing PLS, dopant concentrations (boron and phosphorus) in silicon were first quantified by Tajima [6], who compared the intensity ratio between intrinsic and extrinsic (doped) silicon luminescence components at a temperature of 4.2 K, but only for dopant densities below $1 \times 10^{15}\,\mathrm{cm}^{-3}$ [6]. This range was extended up to a dopant density of $10^{17}\,\mathrm{cm}^{-3}$ in later work by Iwai *et al*. [7], who used the same technique but increased the measurement temperature to 20 K. Liu *et al*. [8] meanwhile demonstrated that it is possible to use the same intensity ratio method to quantify the dopant density at 79 K up to a dopant density of about $10^{18}\,\mathrm{cm}^{-3}$. For more heavily doped ($>10^{18}\,\mathrm{cm}^{-3}$) silicon however, such a method has not been developed, since the shape of the PL spectra depends on a combination of physical phenomena which occur at heavy doping, including band-gap narrowing (BGN), band tail states, degenerate effects (the Fermi level moves into the valence band), and the overlapping of the dopant band with the valence band (for p-type silicon) or conduction band (n-type silicon) [9]. Since the influence of BGN on spectral shape can be very significant with heavy doping, many authors have reported properties of PL spectra at heavy doping and extracted a measure of the amount of BGN by using so-called "line shape analysis" [10]–[12]. Although in the individual physical phenomena mentioned above, each have a different influence upon the shape of the PL spectra, for conditions of heavy doping, the influence of the dopant density is observed via two simple properties of the

Manuscript received April 18, 2017; revised July 11, 2017; accepted August 2, 2017. Date of publication August 22, 2017; date of current version October 19, 2017. This work was supported by the Australian Renewable Energy Agency under Grant RND009. *(Corresponding author: Young-Joon Han.)*

The authors are with the Research School of Engineering, Australian National University, Canberra, A.C.T. 2601, Australia (e-mail: young.han@anu.edu.au; evan.franklin@anu.edu.au; daniel.macdonald@anu.edu.au; hieu.nguyen@anu.edu.au; di.yan@anu.edu.au).

Color versions of one or more of the figures in this paper are available online at http://ieeexplore.ieee.org.

Digital Object Identifier 10.1109/JPHOTOV.2017.2736784

spectra; the shifting of PL peaks and the broadening of the peaks. Roigé *et al*. [13] recently utilized this phenomenon to quantify the dopant density. Their approach was based on room temperature PL spectra, which yield a single, broad luminescence peak, with a shoulder on the long wavelength side which becomes more pronounced as the doping increases. As a result they used an intensity-weighted spectral position of the PL spectra to quantify the dopant density.

The measurement techniques discussed above are restricted to homogenously doped samples, and do not allow dopant density variations to be probed either laterally or depth-wise. These methods are thus limited in application, being unsuitable, for example, for characterization of high-temperature diffused, ion-implanted or laser processed features commonly employed in semiconductor and solar cell fabrication. For inhomogeneous dopant densities, exhibiting variation with depth in heavily doped ($>10^{18}$ cm^{-3}) layers, μ-PLS has been applied by Gundel *et al*. [14] by carefully cross-sectioning and polishing solar cell precursors. This approach is based on the ratio between PL intensities from two PL spectra measurements at room temperature with large and small pinhole sizes of the confocal microscope, rather than analyzing actual PL spectra from a single measurement, and requires careful sample preparation. Recently, qualitative assessments of doping concentrations in heavily doped regions were demonstrated at low temperatures (79 K) via analyzing PL spectra measured perpendicular to the sample surface and requiring no special sample preparation [15], [16]. Courtesy of the low temperature, the spectra reported in these works show, rather than a single dominant luminescence peak, multiple distinct peaks corresponding to emissions from both the heavily doped layer and the underlying silicon substrate.

In this paper, we investigate the feasibility of μ-PLS analysis for empirically determining the key characteristics of doping profiles of heavily p-type boron doped regions, when measured at low temperatures (79 K). This temperature results in sharper and more distinct PL peaks compared to room temperature. Based on a broad range of boron-diffused silicon samples, whose doping profiles are accurately measured via ECV profiling, we correlate PL spectra with doping profiles via the defining parameters of surface dopant density and depth factor. In addition, we demonstrate the effectiveness of this method for localized dopant mapping at the micron scale, by applying it to heavily doped, small-sized features, where we reveal the impact of mask opening size on doping profile characteristics.

II. Experimental Details

The samples investigated in this work were produced via a two-step diffusion process; a quartz tube-furnace boron deposition step, followed by a wet-chemical etch to remove the boron rich layer, and a subsequent high-temperature drive-in step. All samples were prepared on 100 Ω-cm high-resistivity n-type (100) orientation silicon wafers. Sample preparation is described in further detail by Yan and Cuevas in their investigation of BGN in heavily p-doped silicon [17]. A total of 29 different doping profiles are used in this study, with surface dopant densities (N_{surf}) ranging from 3.34×10^{18} to 1.56×10^{20} cm^{-3},

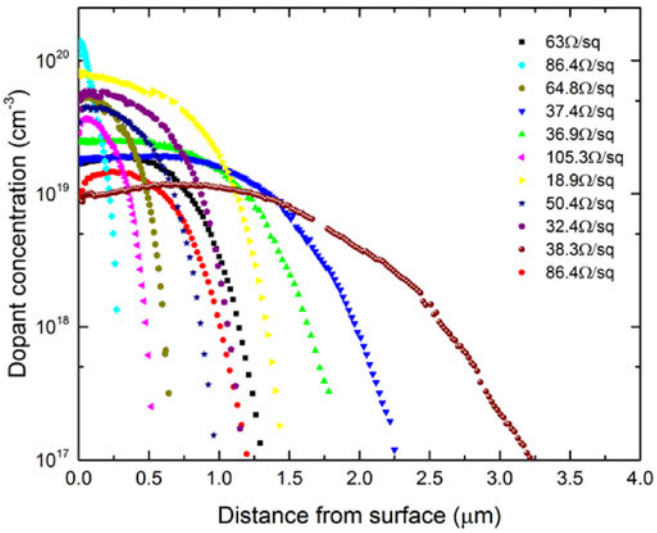

Fig. 1. Doping profiles measured by ECV for a selection of thermally boron-diffused samples used for μ-PLS analysis, with corresponding measured sheet resistances.

and with a range of different diffusion depths between 0.3 and 3.5 μm. A small selection of these doping profiles is depicted in Fig. 1, all sample profiles being determined via calibrated ECV measurements. For each doping profile we subsequently define three key profile characteristics—the peak dopant density, the peak dopant density position, and the depth factor. Since the dopant density for some samples varies considerably in the region immediately below the surface, we also define the surface dopant density, by averaging the dopant densities within 50 nm from the surface. We define the depth factor as employed in the PC1D simulator [18] by fitting a complementary error function (ERFC) or a Gaussian function to these profiles. This is possible since the two-step diffusion process results in a doping profile that can be approximated either by ERFC or Gaussian function, depending upon the process temperature and time of each step, and whether the process can thus be characterized as either a finite or infinite source diffusion [19]. The two functions, described by (1) and (2), respectively, for a dopant density N at depth z, can each be defined by a peak concentration N_p, the depth at which that peak concentration occurs z_p and a depth factor z_f:

$$N(z) = N_p \left\{ 1 - \text{erf}\left[\frac{|z - z_p|}{z_f} \right] \right\} : \text{ ERFC} \tag{1}$$

$$N(z) = N_p \exp\left[\frac{-(z - z_p)^2}{z_f^2} \right] : \text{Gaussian function.} \tag{2}$$

Localized, heavily doped samples for purposes of demonstrating dopant mapping via μ-PLS were also made using the same two-step diffusion process. Features were created via photolithographically defined openings (30, 40, and 50 μm diameter) through a dielectric diffusion mask consisting of a thermally grown silicon dioxide layer ($\sim$30 nm SiO_2) beneath an Low Pressure Chemical Vapor Deposition (LPCVD) stoichiometric silicon nitride layer ($\sim$ 80 nm Si_3N_4). Three differ-

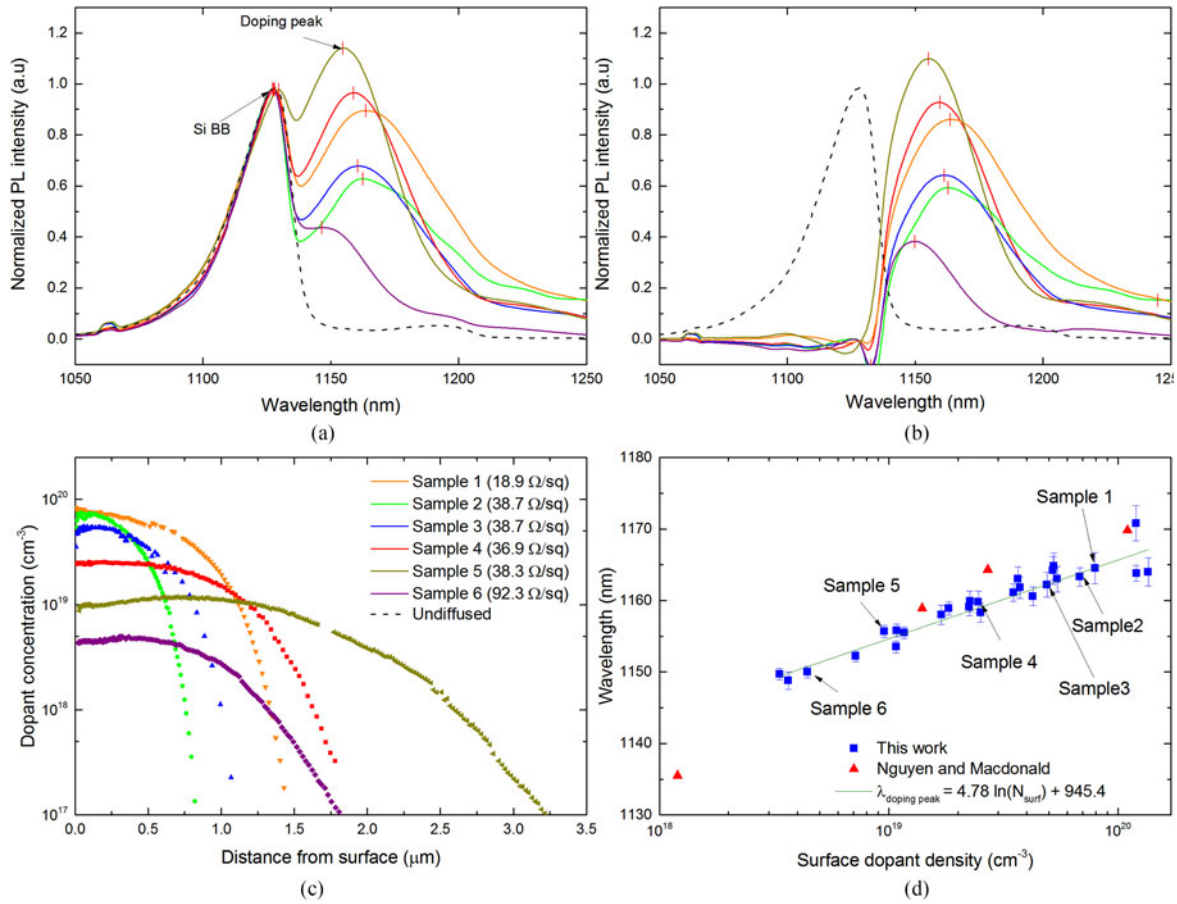

Fig. 2. (a) Normalized PL spectra of a selection of boron-diffused samples with different doping profiles, measured with a 532 nm laser at 79 K. (b) Modified PL spectra by subtracting PL spectra of undiffused Si. (c) The corresponding doping profiles with sheet resistances. (d) Measured wavelengths of the doping peaks as a function of N_{surf} for all samples, along with Nguyen and Macdonald's results [9] measured from homogeneously heavily boron-doped silicon.

ent diffusion recipes were used, yielding light, moderate, and heavy doping, on the same high-resistivity n-type silicon wafers. The resultant profiles were measured via the ECV technique on additional 1 cm $\times$ 1 cm dielectric openings on each patterned wafer. All dielectric masks were subsequently removed in high concentration HF solution prior to measuring PL spectra.

The μ-PLS system employed in this study is a Horiba LABRAM system equipped with confocal optics. For all measurements, the sample temperature was kept at 79 K via a liquid-nitrogen-cooled cryostat. The excitation source was a continuous-wave 532 nm diode-pumped solid state laser, with on-sample incident spot diameter of about 1 μm, achieved using a 50$\times$ objective confocal lens whose numerical aperture is 0.55. The excitation intensity was kept at approximately 134 kW/ cm^2 for all measurements. The absorption depth of the excitation light at 79 K in silicon is around 4.7 μm, calculated from [20], while Auger recombination at such high injection levels restricts carrier diffusion out of the excitation region and thus effectively limits the region of luminescence to a diameter of around 2 μm [21]. A liquid-nitrogen-cooled InGaAs array detector captured the emitted PL spectra, with spectral resolution of 0.4 nm. The spectral response of the entire system was determined with a calibrated tungsten-halogen lamp. In order to compare PL spectra of different samples, the intensity of PL spectra were normalized to the silicon band–band peak ($\sim$1128 nm) from the underlying lightly doped substrate. All samples measured in this work have planar surfaces formed via saw-damage etching in 25% tetramethylammonium hydroxide solution, without any passivation films present.

Since the measured PL spectra contain the silicon substrate band-to-band peak as well as the doping luminescence peak of interest, subsequent to each measurement the PL spectra measured from an undiffused control silicon were subtracted to more easily resolve the luminescence peak from the heavily doped layers. This is illustrated in Fig. 2(b). For the locally diffused samples, a 2-D scan mapping with 2 μm spatial resolution was conducted, and the full PL spectra measured and analyzed at each point, to characterize the locally doped regions in terms of N_{surf} and z_f across the entire feature.

III. Results and Discussion

A. Determination of N_{surf} Via Doping Peak Wavelength

Measured PL spectra, subtracted PL spectra showing only components from the heavily doped layers, and the corresponding doping profiles, measured via ECV, of a selection of samples are depicted in Fig. 2(a)–(c), respectively. Fig. 2(a) clearly shows two distinct peaks, at around 1130 and 1160 nm, corresponding

to the radiative recombination of the underlying silicon substrate (Si BB) and the recombination in the heavily doped silicon layer (doping peak), respectively. The spectrum measured from an undiffused sample is also included for comparison. This spectrum is consistent for any undiffused silicon sample, and additionally represents the emission spectrum from the excited substrate region immediately below the diffused layer in our samples.

Since the doping profiles are not homogenous with depth, the detected PL signal is a weighted sum over the individual spectra emitted from the varying doping concentrations, resulting in a broadening of the peak. Courtesy of the fact that the excitation irradiance is absorbed most strongly near the sample surface, and the high intensity incident irradiation which ensures an Auger-dominated carrier lifetime in the underlying substrate, the generation, and recombination of carriers is confined to near the front surface. Furthermore, emissions from nearer the front surface have a higher probability of falling within the detection angle of the detector. As a result, PL from recombination just below the surface, in the region of heaviest doping, dominates over PL from further below the surface. Therefore, we can regard the wavelength of the doping peak as a proxy for the surface dopant density. To more clearly resolve the doping peak, particularly useful for light and/or shallow doped layers such as sample 6, we subtract the normalized spectra for an undiffused sample and again identify the wavelength of the PL peak, corresponding to the dominant surface dopant density.

The hypothesis that the wavelength of the doping peak is a proxy for the surface dopant density is verified in Fig. 2(d), plotting for all samples the wavelength corresponding to the doping peak as a function of N_{surf}. Error bars indicate the range of wavelengths having PL intensities larger than 99.5% of the doping peak intensity, thus representing the uncertainty in determining the exact location of the peak. Nguyen and Macdonald's results [9], measured under similar conditions on homogeneously heavily boron-doped silicon wafers, also support our conclusion by showing close agreement with our measured values. Our data clearly reveal that the wavelength of the doping peak increases with increasing N_{surf}, displaying a consistent linear relationship on a semilog plot over the range of interest. We can thus establish a simple "calibration curve" for estimating N_{surf} from the wavelength of the doping peak. The relationship, which can subsequently be applied to any boron diffused surfaces if PLS measurements are taken under similar conditions, is also shown in Fig. 2(d), and is described by

$$\lambda_{\text{doping peak}} = (4.78 \pm 0.25)\ \ln(N_{\text{surf}}) + (945.4\ \pm 10.9)\,. \tag{3}$$

We observe that the amount of peak shifting toward longer wavelength does not match what might be anticipated from simple application of theoretical BGN models, thus serving to highlight the complexity of the PL spectra modification which occurs with heavy doping. Based on Schenk's BGN model [22], when the dopant density increases from $\sim 3 \times 10^{18}$ to $\sim 1 \times 10^{20}\,\text{cm}^{-3}$, a theoretical band gap shrinkage of around 60 meV occurs, whereas the peak shifting we observed results in an apparent narrowing of only about 20 meV ($\Delta\lambda \sim 20\,\text{nm}$). Much less peak shifting is observed than predicted by the BGN model alone due to the counter influence of the degenerate effect which occurs in silicon at very high doping [9]. Increasing the dopant density obviously causes more BGN, resulting in the peak shifting toward longer wavelength. However, in degenerate silicon, the Fermi level moves into the band, not only shifting the spectra to shorter wavelength (higher energy), but also broadening all PLS features [9]. This broadening effect of degenerate silicon is also observable in Fig. 2(b), where the width of the doping peak is observed to increase with N_{surf}. Therefore, since most of the samples investigated in this work experience the competing influences of BGN and the degenerate effects under the conditions required for PL measurement, a separate study would be required to apply a theoretical fit to our data. We thus rely upon the empirical relationship established in this work for the further analysis of doped features.

B. Determination of z_f Via Doping Peak Intensity

We have established that the position of the doping peak corresponds directly to the surface dopant density, yet we also observe in Fig. 2(b) that for our samples the relative intensity of the doping peak varies considerably with the profile depth. The doping peak corresponds to emissions from the heavily doped subsurface region while the silicon band-to-band peak corresponds to emissions from the underlying substrate. The ratio of these intensities, therefore, reflects how much emission originates from the heavily doped layer compared to the substrate. Since the depth of the excitation region is largely fixed according to the absorption depth of the excitation wavelength, this ratio could, therefore, represent a measure of the depth of the heavily diffused layer. Furthermore, the doped layer has a smooth transition between high and low doping, rather than a step change, and so rather than defining a simple doped layer depth we instead apply a commonly used depth metric, the depth factor (z_f), for diffused layers.

After confirming that the doping profiles of the investigated samples all show a good fit to a Gaussian function, we have fitted the depth factor from the Gaussian function for all samples and attempted to correlate this value with the normalized intensity of the doping peak. The Gaussian fit is consistent with expectations, given that the boron source glass is removed prior to the final thermal drive-in process in each case, meaning the dopant source is finite. A consistent fit between doping peak intensity and depth factor would mean that we can use PL spectral analysis to not only estimate the diffusion depth, but also reconstruct the doping profile based on the relationship already established for the surface dopant density, assuming the profile follows a Gaussian shape. We also observe that the reconstructed profile cannot include the term of z_p, required for a profile with peak doping occurring at a position considerably below the surface, as there is currently no reliable means of extracting the z_p component from the PL spectra analysis.

Fig. 3(a) plots the normalized doping peak intensity versus the depth factor for all samples. Generally speaking, the doping peak intensity increases monotonically with diffused layer depth, as anticipated from theoretical considerations. However, it is evident from this dataset that a quite wide spread in depth

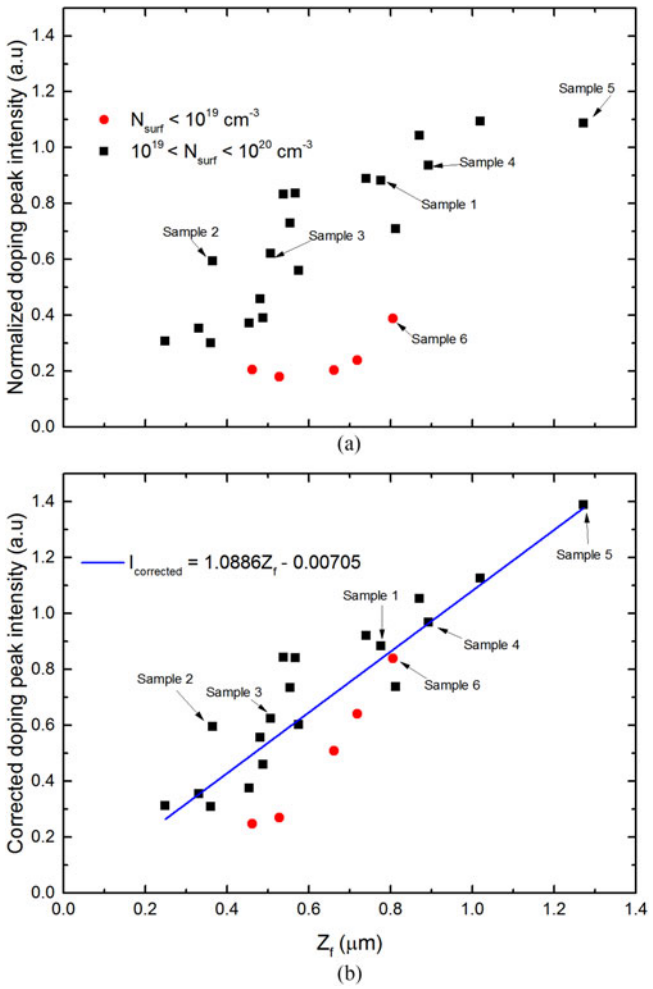

Fig. 3. Normalized doping peak intensity as a function of depth factor, (a) without any correction, and (b) including a correction for the effect of incomplete ionization on PL intensity. Representative samples shown in Fig. 2 are also labeled accordingly.

factor at similar levels of doping peak intensity is observed. In addition, lightly doped samples ($N_{\text{surf}} < 1 \times 10^{19}\,\text{cm}^{-3}$) show a much larger discrepancy compared to the other samples. For example, in Fig. 2, sample 6 shows a relatively deep profile compared to the other samples, whilst having the lowest doping peak intensity.

This is due to the fact that incomplete dopant ionization is significant for lightly doped samples ($N_{\text{surf}} < 1 \times 10^{19}\,\text{cm}^{-3}$), and incomplete ionization is also more pronounced at the lower temperature at which our PLS measurements occur [23], [24]. The absolute PL intensity for the heavily diffused layer is related to the ionized dopant density, since the PL intensity is proportional to the np product or in our case $\sim(N_A + \Delta n) \times \Delta n$, where N_A is the ionized dopant density and Δn is the excess carrier density [25]. As the PL spectra of diffused layers are primarily influenced by N_{surf}, any sample where significant incomplete ionization occurs under the PLS measurement conditions will exhibit an overall reduced PL intensity, at those wavelengths corresponding to the doping-induced BGN, compared to that which might be anticipated by consideration alone of the measured N_{surf} at room temperature. The reduction in PL intensity will correspond approximately to the fraction of nonionization which occurs near the surface during the PLS measurement conditions. This interpretation is supported by comparing samples 1, 4, and 6 in Fig. 2. Although all samples have a similar profile depth, sample 6 shows a much lower doping peak intensity than the other two samples, since sample 6 has only about 46% of dopants activated near the surface at 79 K, according to our calculations using the method described by Altermatt *et al.* [23], [24]. Therefore, it is necessary to consider the effect of the incomplete ionization, calculated for each measured N_{surf}, on the PL intensity when correlating the depth factor to the PL intensity.

Fig. 3(b) plots again the normalized doping peak intensity against depth factor, but with a simple division of the raw PL intensity by the fraction of ionization for each sample. The result shows an improved linear relationship between the doping peak intensity and the depth factor across all sample types, compared to Fig. 3(a). In particular, the measurements for the lightly doped samples now follow more closely the main linear trend. However, there is still quite a wide spread, most likely due to uncertainty associated with variable excess carrier density (Δn) between samples, leading to an unpredictable np product, and also due to nonionization fractions which are not fixed for any given sample but rather which vary with depth. Meanwhile, an accurate estimation of the value of Δn is very difficult since it not only depends on the generation profile (excitation intensity), but also on the electronic properties of the substrate, diffused layer, and surface. Particularly, the unpassivated surface conditions incur a significant change in Δn near the surface, so that shallower profiles are more heavily influenced by surface conditions. Hence, individual samples would have a different value of Δn even under the same excitation conditions, which in turn influences the relative intensity of the doping peak and the substrate band-to-band peak. Therefore, if we could estimate an accurate value of Δn for each individual sample, we could deduce the depth factor of the profile more precisely. Nonetheless, we establish here the simple linear calibration curve, as described in Fig. 3(b) and (4), between the corrected doping peak intensity and the depth factor for the remainder of our work, in order to approximately reconstruct the doping profiles from PLS measurements:

$$I_{\text{corrected}} = (1.0886 \pm 0.128)\ z_f - (0.00705 \pm 0.08562)\,. \tag{4}$$

This calibration curve is also valid only when the PLS measurement is conducted under the conditions similar to those stated in this study.

C. Application on Locally Diffused Samples

We now examine the validity of this characterization method to reconstruct doping profiles, and demonstrate the potential of dopant mapping via μ-PLS, by investigating locally diffused regions. Fig. 4 plots the normalized and subtracted PL spectra of locally diffused samples with the corresponding doping profiles, measured at large-area regions uniformly diffused through $1\,\text{cm} \times 1\,\text{cm}$ dielectric openings. Three different profiles are

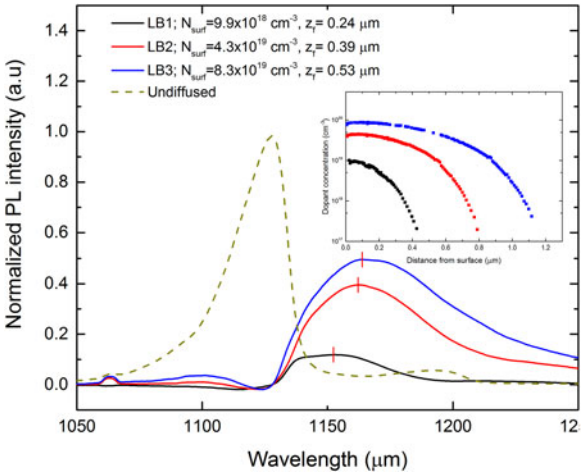

Fig. 4. Normalized and subtracted PL spectra of locally diffused samples, labeled as LB1–3 with N_{surf} and z_f, measured at the center region of diffused 1 cm × 1 cm with a 532 nm laser at 79 K. The corresponding profiles are shown in the inset.

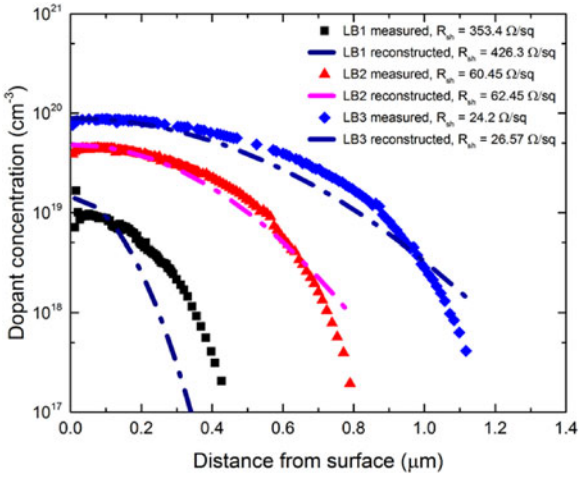

Fig. 5. Measured and reconstructed doping profiles, used for localized diffusions, with corresponding sheet resistances.

prepared for light (labeled as LB1 in Fig. 4), moderate (LB2), and heavy (LB3) doping cases, showing distinct N_{surf} and diffusion depths. Corresponding sheet resistances are 353, 60, and 24 Ω/sq, respectively.

Based on the profiles, we could expect three different wavelengths and intensities of the doping peaks from the PL spectra, as confirmed in Fig. 4. Wavelengths of doping peaks for LB1–3 samples are about 1156, 1162, and 1165 nm, respectively. Based on (3), the corresponding N_{surf} are approximately 1.4×10^{19}, 4.8×10^{19}, and 8.9×10^{19} cm^{-3}, and show close agreement to the measured values. In addition, the normalized doping peak intensities for each sample are about 0.12, 0.4, and 0.5, respectively. Using (4) after considering the impact of incomplete ionization of the dopants on the raw doping peak intensity, values of z_f are estimated to be about 0.14, 0.37, and 0.47 μm. Thus, we can, from PLS measurements alone, reconstruct the doping profiles of these diffused samples, based on our calculated values for N_{surf} and z_f. The value of z_p is assumed to be zero. Substituting all parameters in (2), the reconstructed doping profiles are plotted in Fig. 5, with the corresponding calculated sheet resistances. Although the reconstructed curves do not perfectly match the measured ECV curves, particularly for the very lightly doped sample, the agreement is nevertheless reasonable.

We now conduct 2-D mappings of N_{surf} (see Fig. 6) and z_f (see Fig. 7) with 2 μm spatial resolution over locally diffused regions through photolithographically defined 30, 40, and 50 μm diameter circular openings on dielectric masks, by measuring and analyzing PL spectra at each point. Comparing the images row by row in each figure allows us to observe the effect of different profiles for LB1–3, while the effect of the mask size can be seen by comparing column by column.

In Fig. 6, we again distinctly observe three values of N_{surf} for each profile, at about 1.2×10^{19}, 4.8×10^{19}, and 9×10^{19} cm^{-3}. In addition, these samples show good uniformity over the diffusion area, regardless of the size of the dielectric mask openings, and also exhibit distinct and sharp edges. This is to be expected for a diffusion that occurs into a region which

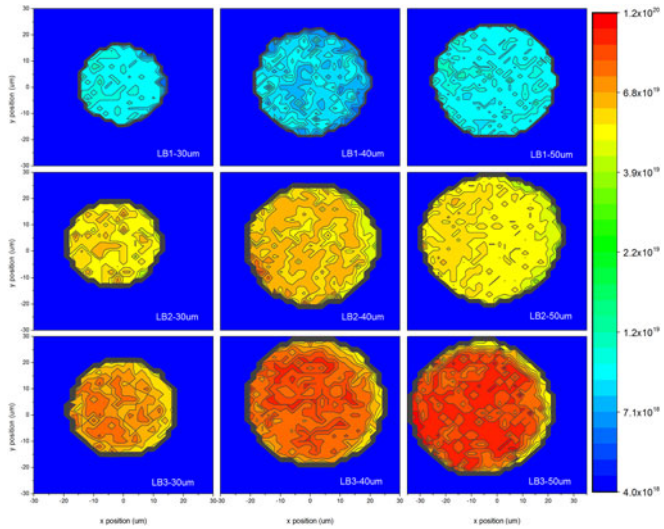

Fig. 6. 2-D scanned maps of N_{surf}, for locally diffused samples through 30, 40, and 50 μm dielectric mask openings.

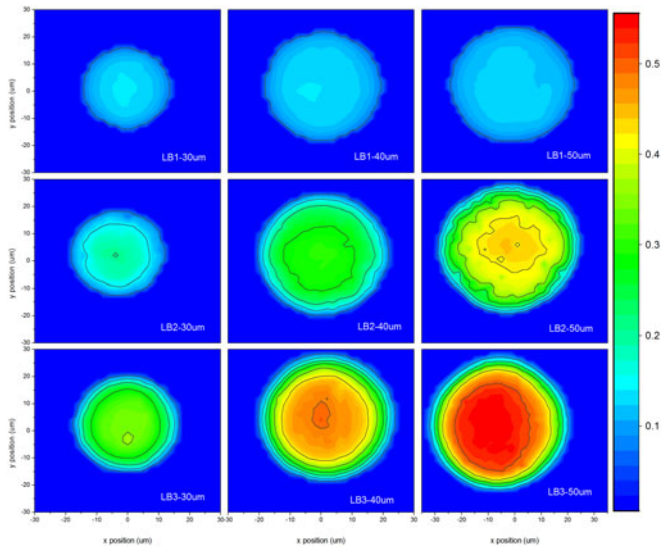

Fig. 7. 2-D scanned maps of z_f, for locally diffused samples through 30, 40, and 50 μm dielectric mask openings.

has itself been created by a well-defined mask edge, and serves to demonstrate the powerful capability of accurate 2-D surface dopant density mapping via this method. Interestingly, we do, however, note that the dopant density is markedly lower over a distance of a few microns from one edge (particularly evident for the more heavily doped samples), and we attribute this to gas-flow dynamics associated with the deposition of the boron-rich glass during the tube furnace diffusion process.

In contrast to our observation of uniform surface dopant density, the maps of the calculated depth factor in Fig. 7 show a notable pattern. When comparing light, medium, and heavy diffusions, the mapped depth factor generally increases as expected from the ECV profile measurements, and at the center of the larger (50 μm diameter) features does give a reliable measure of diffusion depth. However, an unexpected and considerable variation in the implied depth factor across the region of the masked diffusions is observed. We observe a decreasing depth factor value near the edges of the diffused areas. This could in principle be due to the dopant diffusion process itself, which produces some lateral and diagonal movement of dopants into regions around the perimeter of the masked region. However, the extent of the lateral variation observed, extending some 10 μm from the edge of the features, is inconsistent with impurity diffusion processes. Hence, this observation is most likely associated with a measurement artifact, in particular to lateral carrier diffusion, which results in a larger than anticipated "detection volume" from which luminescence is detected. This results in a carrier smearing effect, where the intensity of the detected PL spectra can be influenced by the undiffused region surrounding the heavily doped features. Although the measurement conditions, particularly the high excitation power, have been chosen to restrict the carrier diffusion length and confine the detection volume as much as possible, the precise dimensions of the detection volume are difficult to estimate, due to limited knowledge of Auger recombination rates and carrier mobilities at these low temperatures. Nevertheless, our observations suggest that carrier smearing currently places a limit on the accuracy of this approach to determine the doping depth for small features. We note, however, that our approach for mapping the surface dopant density is not limited in the same manner, since it depends only on the position of the doping peak, rather than its intensity.

To further investigate the effect of carrier smearing on diffusion depth profiling, we measured and analyzed PL spectra using different excitation intensities from 74 to 320 kW/ cm^2. This range of excitation intensities results in different injection levels and therefore different Auger recombination-limited detection volumes. This should in turn result in a difference in the carrier smearing effect and hence a difference in the implied diffusion depth profile near the edge of heavily diffused features. Fig. 8(a) plots the normalized doping peak intensity of a horizontal section across 2-D maps of the LB3-40 μm sample, for the three different excitation intensities. Lower excitation intensity increases the relative doping peak intensity, as shown by Nguyen *et al*. [15] due to different dependences of the np product on excitation intensity for the heavily diffused and lightly doped substrate layers: the undiffused layers respond to Δn quadratically, while the diffused layers respond to Δn linearly.

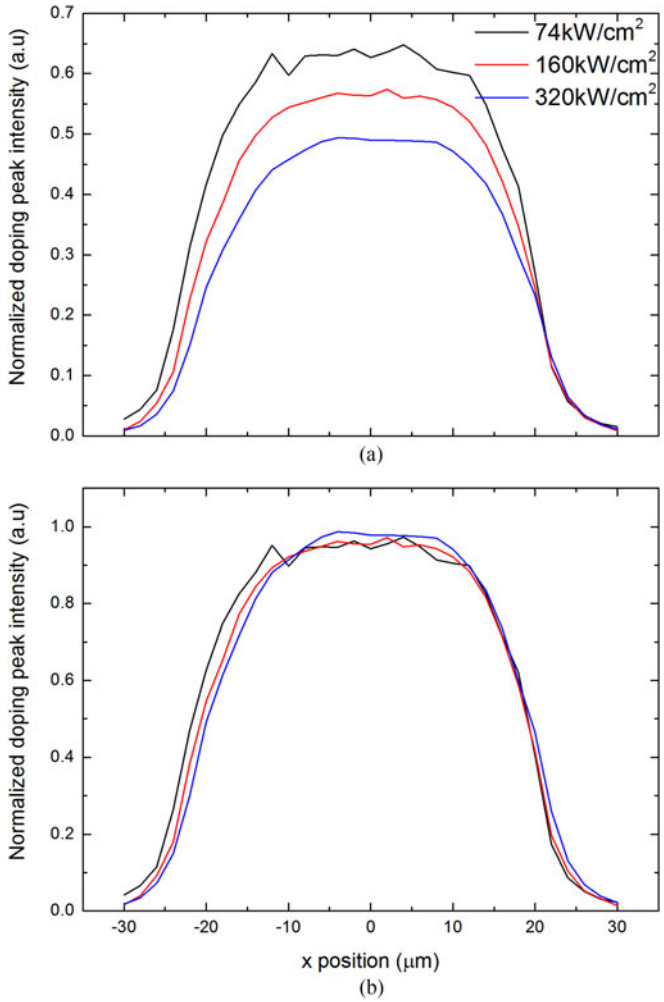

Fig. 8. (a) Horizontal section of 2-D map of LB3-40 μm sample's doping peak intensity, measured with different excitation intensity (74, 160, 320 kW/ cm^2), and (b) normalized to 1 for the comparison.

However, the lateral carrier diffusion length does not appear to change significantly under this variation of Δn. As can be seen in Fig. 8(b), all three normalized horizontal lines are similar, not showing any significant differences between measurements in the vicinity of the edge of the heavily doped feature. This is possibly due to very short carrier lifetime conditions in the diffused layer (unpassivated surface and low temperature) regardless of carrier injection levels, or simply that this range of injection levels does not incur much change in carrier lifetime. Despite this result not showing clearly the impact of lateral carrier diffusion on our analysis technique, this effect still seems most likely to be the cause of the observed reduction in calculated depth factor near the edges of heavily doped features. We, therefore, conclude that the analysis method developed in this work can be used to reliably determine the depth factor of boron diffused surfaces, but has limited accuracy around the edges of locally doped features.

IV. Conclusion

We have investigated the potential use of low temperature μ-PLS measurements to determine the inhomogeneous Gaussian function type doping profiles, in terms of surface

dopant density and depth factor, for heavily p-type boron diffused silicon wafers. Measured PL spectra were normalized to the underlying Si band–band peak, and the PL spectrum of an undiffused control wafer was subtracted to resolve the heavy-doping peak. We found that the wavelength of the doping peak and surface dopant density have a simple linear relationship on a semilog plot, and established a calibration curve which can be applied to estimate the surface dopant density in the range 5×10^{18} to $1 \times 10^{20}\,\mathrm{cm}^{-3}$ from the doping peak wavelength alone. Another calibration curve is established for determining the depth factor, after considering incomplete dopant ionization, and can be applied for diffusion depths up to at least 3–4 μm. We demonstrate using these two calibration curves that we are able to reconstruct a boron diffusion profile based on the estimated surface dopant density and depth factor determined via PLS spectral analysis only. We note, however, that an accurate parameterization of the excess carrier density during PLS measurement would allow us to quantify the depth factor with greater precision. We also show 2-D mapping of the surface dopant density and the depth factor by applying this method at each point with 2 μm resolution on locally diffused samples with small feature sizes. A uniform and sharply defined surface dopant density is observed regardless of diffusion feature size, but the calculated depth factor varies significantly according to the size of the feature, being observed to reduce as the perimeter of a feature is approached. We attribute this depth factor limitation near feature edges to considerable lateral carrier diffusion, which results in carrier smearing and an unreliable calculation of diffusion depth within a distance of around 10–15 μm from feature edges.

REFERENCES

[1] J. Zhao, A. Wang, M. A. Green, and F. Ferrazza, "19.8% efficient "honeycomb" textured multicrystalline and 24.4% monocrystalline silicon solar cells," *Appl. Phys. Lett.*, vol. 73, pp. 1991–1993, 1998.

[2] E. Franklin *et al.*, "Design, fabrication and characterisation of a 24.4% efficient interdigitated back contact solar cell," *Prog. Photovolt.: Res. Appl.*, vol. 24, pp. 411–427, 2016.

[3] E. Peiner, A. Schlachetzki, and D. Krüger, "Doping profile analysis in Si by electrochemical capacitance-voltage measurements," *J. Electrochem. Soc.*, vol. 142, pp. 576–580, Feb. 1995.

[4] A. Benninghoven, F. G. Rudenauer, and H. W. Werner, *Secondary Ion Mass Spectrometry: Basic Concepts, Instrumental Aspects, Applications and Trends*. New York, NY, USA: Wiley, 1987.

[5] C. J. Park, K. J. Kim, M. J. Cha, and D. S. Lee, "Determination of boron in uniformly-doped silicon thin films by isotope dilution inductively coupled plasma mass spectrometry," *Analyst*, vol. 125, pp. 493–497, 2000.

[6] M. Tajima, "Determination of boron and phosphorus concentration in silicon by photoluminescence analysis," *Appl. Phys. Lett.*, vol. 32, pp. 719–721, 1978.

[7] T. Iwai, M. Tajima, and A. Ogura, "Quantitative analysis of impurities in solar-grade Si by photoluminescence spectroscopy around 20 K," *Phys. Status Solidi C*, vol. 8, pp. 792–795, 2011.

[8] A. Liu, H. T. Nguyen, and D. Macdonald, "Quantifying boron and phosphorous dopant concentrations in silicon from photoluminescence spectroscopy at 79 K," *Phys. Status Solidi A*, vol. 213, pp. 3029–3032, 2016.

[9] H. T. Nguyen and D. Macdonald, "On the composition of luminescence spectra from heavily doped p-type silicon under low and high excitation," *J. Lumin.*, vol. 181, pp. 223–229, 2017.

[10] J. Wagner, "Photoluminescence and excitation spectroscopy in heavily doped n- and p-type silicon," *Phys. Rev. B*, vol. 29, pp. 2002–2009, 1984.

[11] J. Wagner, "Band-gap narrowing in heavily doped silicon at 20 and 300 K studied by photoluminescence," *Phys. Rev. B*, vol. 32, pp. 1323–1325, 1985.

[12] W. P. Dumke, "Band-gap narrowing from luminescence in p-type Si," *J. Appl. Phys.*, vol. 54, pp. 3200–3202, 1983.

[13] A. Roigé *et al.*, "Effects of photon reabsorption phenomena in confocal micro-photoluminescence measurements in crystalline silicon," *J. Appl. Phys.*, vol. 121, 2017, Art. no. 063101.

[14] P. Gundel *et al.*, "Micro-spectroscopy on silicon wafers and solar cells," *Nanoscale Res. Lett.*, vol. 6, pp. 1–8, 2011.

[15] H. T. Nguyen *et al.*, "Micro-photoluminescence spectroscopy on heavily-doped layers of silicon solar cells," *Phys. Status Solidi R*, vol. 9, pp. 230–235, 2015.

[16] Y.-J. Han *et al.*, "Low-temperature micro-photoluminescence spectroscopy on laser-doped silicon with different surface conditions," *Appl. Phys. A*, vol. 122, pp. 1–10, 2016.

[17] D. Yan and A. Cuevas, "Empirical determination of the energy band gap narrowing in p+ silicon heavily doped with boron," *J. Appl. Phys.*, vol. 116, 2014, Art. no. 194505.

[18] D. A. Clugston and P. A. Basore, "PC1D version 5: 32-bit solar cell modeling on personal computers," in *Proc. 26th IEEE Photovolt. Spec. Conf., Conf. Rec.*, 1997, pp. 207–210.

[19] R. C. Jaeger, *Introduction to Microelectronic Fabrication*, vol. 5. Upper Saddle River, NJ, USA: Prentice-Hall, 2002.

[20] M. A. Green, "Self-consistent optical parameters of intrinsic silicon at 300 K including temperature coefficients," *Sol. Energy Mater. Sol. Cells*, vol. 92, pp. 1305–1310, 2008.

[21] P. Gundel, F. D. Heinz, M. C. Schubert, J. A. Giesecke, and W. Warta, "Quantitative carrier lifetime measurement with micron resolution," *J. Appl. Phys.*, vol. 108, 2010, Art. no. 033705.

[22] A. Schenk, "Finite-temperature full random-phase approximation model of band gap narrowing for silicon device simulation," *J. Appl. Phys.*, vol. 84, pp. 3684–3695, 1998.

[23] P. P. Altermatt, A. Schenk, and G. Heiser, "A simulation model for the density of states and for incomplete ionization in crystalline silicon. I. Establishing the model in Si:P," *J. Appl. Phys.*, vol. 100, 2006, Art. no. 113714.

[24] P. P. Altermatt, A. Schenk, B. Schmithüsen, and G. Heiser, "A simulation model for the density of states and for incomplete ionization in crystalline silicon. II. Investigation of Si:As and Si:B and usage in device simulation," *J. Appl. Phys.*, vol. 100, 2006, Art. no. 113715.

[25] H. T. Nguyen, F. E. Rougieux, S. C. Baker-Finch, and D. Macdonald, "Impact of carrier profile and rear-side reflection on photoluminescence spectra in planar crystalline silicon wafers at different temperatures," *IEEE J. Photovolt.*, vol. 5, no. 1, pp. 77–81, Jan. 2015.

Authors' photographs and biographies not available at the time of publication.